# Trophic level decoupling drives future change in phytoplankton bloom phenology

**Ryohei Yamaguchi** ( ryamaguchi@pusan.ac.kr )
Center for Climate Physics, Institute for Basic Science https://orcid.org/0000-0002-7800-5798
**Keith Rodgers**
Center for Climate Physics, Institute for Basic Science
**Karl Stein**
Center for Climate Physics, Institute for Basic Science
**Axel Timmermann**
Pusan National University https://orcid.org/0000-0003-0657-2969
**Sarah Schlunegger**
Princeton University https://orcid.org/0000-0002-6668-9088
**Daniele Bianchi**
University of California Los Angeles https://orcid.org/0000-0002-6621-0858
**John Dunne**
Geophysical Fluid Dynamics Laboratory https://orcid.org/0000-0002-8794-0489
**Richard Slater**
Princeton University

**Article**

**Keywords:** trophic level decoupling, phytoplankton bloom phenology, anthropogenic climate change, marine ecosystems

**Posted Date:** June 21st, 2021

**DOI:** https://doi.org/10.21203/rs.3.rs-604906/v1



**Version of Record:** A version of this preprint was published at Nature Climate Change on May 9th, 2022.
See the published version at https://doi.org/10.1038/s41558-022-01353-1.

# Trophic level decoupling drives future change in phytoplankton bloom phenology

Ryohei Yamaguchi[1,2 *], Keith B. Rodgers[1,2], Karl J. Stein[1,2], Axel Timmermann[1,2], Sarah Schlunegger[3], Daniele Bianchi[4], John P. Dunne[5], and Richard D. Slater[3]

[1] *Center for Climate Physics, Institute for Basic Science, Busan, South Korea*

[2] *Pusan National University, Busan, South Korea*

[3] *AOS Program, Princeton University, NJ, United States*

[4] *University of California, Los Angeles, CA, United States*

[5] *NOAA Geophysical Fluid Dynamics Laboratory, NJ, United States*

***** Corresponding author: Ryohei Yamaguchi (ryamaguchi@pusan.ac.kr)

In preparation for Nature Climate Change

9, June 2021

This manuscript includes 3002 words in main text with 5 figures and captions.

# Abstract (147 words, 150 words limit)

Anthropogenic climate change is affecting marine ecosystems by altering the strength of phytoplankton blooms and driving shifts in the seasonality (phenology) of productivity. Here, we analyze a new 30-member Large Ensemble of climate change projections to quantify the sensitivity of phytoplankton bloom phenology (initiation, peak timing, and net growth period length) to anthropogenic forcing. Forced changes in the duration of net growth vary widely across the global ocean, with high latitudes experiencing a reduction of up to one month, and the tropics and subtropics experiencing an extension of up to one month. Changes in duration reflect shifts in both bloom initiation and peak bloom timing, which result from subtle decoupling between phytoplankton growth and zooplankton predation driven by temperature, nutrients and light variations. Changes in bloom strength and timing will alter the flow of energy in the marine ecosystem, with implications for higher trophic levels and fisheries.

# Main text

Marine primary productivity, the sum of organic carbon fixed by microbes in the ocean, is a fundamental aspect of the Earth system. The potential for climate change to have deleterious impacts on marine primary productivity has received significant attention, with coordinated efforts to understand and predict the long-term production capacity of marine ecosystems. This long-term capacity has implications for the global food supply, an important consideration given expected population growth, and for the ocean's capacity to sequester anthropogenic carbon. In addition to understanding the future changes in mean productivity, it is important to also assess whether the seasonal cycle of productivity can change in response to anthropogenic forcing, as shifts in phenology may also have large implications for natural and human systems. For example, changes in the timing of energy fixation at the base of the food web may affect fisheries and food security by de-synchronizing energy transfer to higher trophic levels[1–3]. Phenology changes may also have impacts on net annual oceanic fixation of inorganic carbon, which affects net ocean anthropogenic $CO_2$ uptake and acidification[4–6].

There is broad consensus that the terrestrial biosphere is projected to experience longer growing seasons under anthropogenic forcing[7–11]. However, there is less consensus regarding the drivers of marine phenology changes, compared to the terrestrial analogue. Over most of the extra-tropical oceans, the seasonal cycle of productivity is dominated by phytoplankton blooms, which have been shown to be sensitive to future warming[12]. Previous studies have suggested that the onsets of bloom and growing season defined by indicators of ocean phytoplankton abundance and productivity (e.g., chlorophyll concentration (Chl) and net primary production (NPP)) have already shifted earlier in phase[1,13–16] and will continue to shift in the near future[2,12,17,18], especially at high latitudes. Lack of consensus about the future of the

phytoplankton phenology, however, partially stems from the complexity and diversity of environmental drivers (temperature, light, nutrient availability, grazing pressure, among others) that trigger and sustain phytoplankton blooms[19,20], and underlying uncertainty in the forced response of these drivers[21].

Early efforts to explain climate-driven phenology shifts relied on the Sverdrup critical depth paradigm[22] to argue that surface warming will drive an earlier onset of spring stratification, thereby modulating phytoplankton bloom timing as a 'bottom-up" control[2,17]. Alternatively, recent studies have emphasized the importance of a more diverse set of mechanisms that include reduced predation by zooplankton and a subsequent increase in phytoplankton growth[19,23–26], constituting "top-down" controls. Given that the pertinent drivers tend to covary, simple correlation analysis cannot be expected to deconvolve the underlying mechanisms.

In this study, we use the accumulation rate of surface Chl to define the phytoplankton bloom period[27] (i.e., net growth period) and calculate the balance for change in the accumulation rate to quantitatively attribute the projected phytoplankton phenological shifts (see Methods). This methodology enables us to disentangle the complexity of the system and gain insights into the different underlying mechanisms and their response to climate change driven by expected both physical and biological environmental drivers' changes[28–30].

Despite strong anthropogenic changes in many ocean properties impacting primary production (e.g. temperature, mixing), analyses of large ensemble Earth system model simulations has shown that forced trends (anthropogenic signals) in biological variables (e.g., Chl and NPP) are relatively subtle, taking many decades to statistically 'emerge' above background climate variability[21]. This underscores the utility, if not necessity, of a large ensemble framework for

isolating and attributing forced trends in marine biological variables. Here, we leverage daily surface Chl data and other related variables from the 30-member Large Ensemble with the Geophysical Fluid Dynamics Laboratory Earth System Model 2 (GFDL-ESM2M[31–33]) under a high emission scenario (historical/RCP8.5) to investigate future changes in phytoplankton phenology (Fig. 1). GFDL's ESM2M has three phytoplankton groups and one allometric/diagnostic zooplankton class, and explicitly represents a prognostic chlorophyll-carbon ratio (Chl:C; more precisely, a flexible chlorophyll to nitrogen ratio, see Supplementary note). The model realistically represents the main features of the seasonal cycle of sea surface Chl[34], i.e. the timing of phytoplankton blooms, as documented by the comparison with satellite records (Fig. S1).

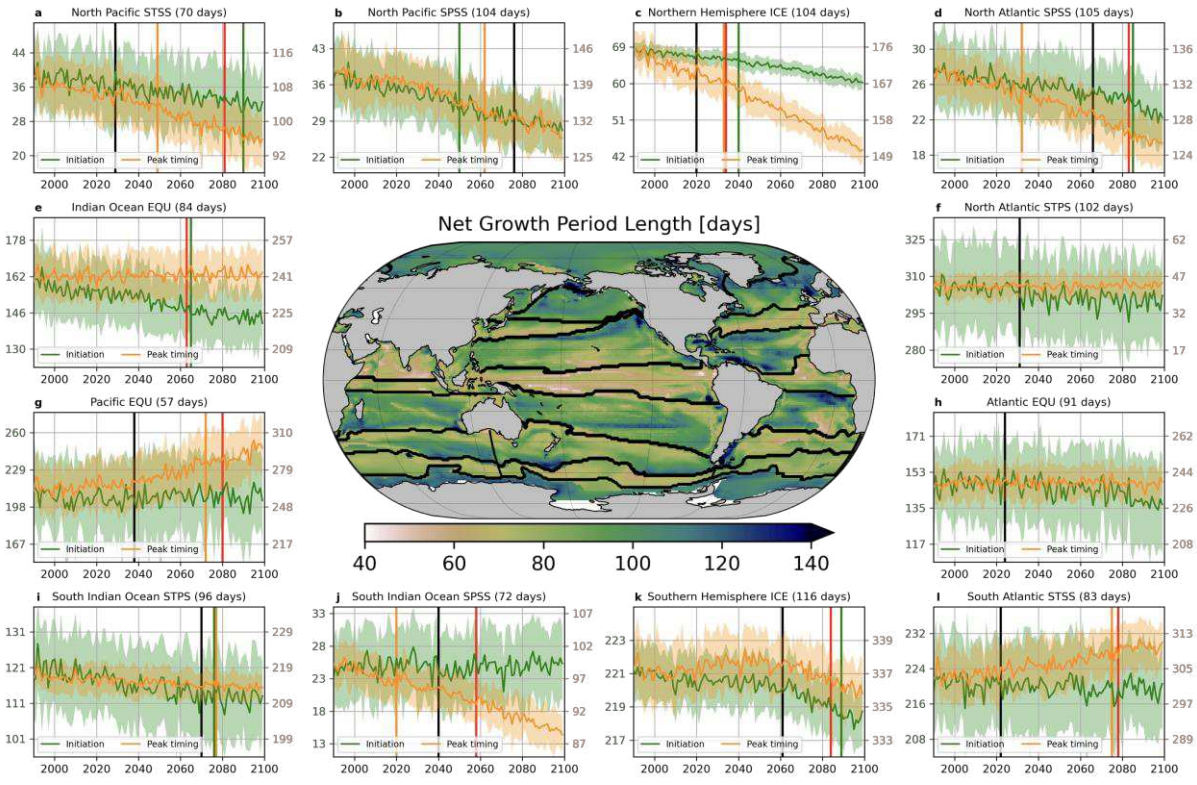


**Figure 1. Climatological net growing period and anthropogenic shifts in the bloom initiation and peak.** Ensemble mean climatology (1990–2020) of the ocean net growth period length (center, [days]) and biome-mean time series of phytoplankton bloom initiation (green lines, left axes, [day of the year]) and peak timing (orange lines, right axes, [day of the year]). Black contours superimposed on the map indicate the biome[35] boundaries used in this study. Each basin except for the North Indian Ocean has ice (ICE), subpolar seasonally stratified

(SPSS), subtropical seasonally stratified (STSS), subtropical permanently stratified (STPS), and equatorial (EQU) biomes in order from the pole. Time of emergence (ToE) with respect to 1990 of biome-aggregated time series of bloom magnitude, net growth period length, bloom peak timing, and bloom initiation are shown in black, red, orange, and green vertical lines, respectively. If there is no corresponding vertical line, the metric is not emergent by the end of simulation period. Full time series and detailed biome definition can be seen in Fig. S2. Shadings in time series indicate the range of one standard deviation of 30 ensemble members. The numbers in parentheses next to the biome names gives the biome-mean climatology of net growth period length.

## Future projection of bloom phenology

We begin by examining the length of the net growth period, defined as the number of days between the initiation of the bloom and its peak (see Methods). This definition is suited to blooms in the mid- to high-latitudes, but in the non bloom-forming tropics it only represents one aspect of the seasonal cycle. The spatial pattern of net growth period length (Fig. 1) aligns qualitatively well with biome patterns, defined by ocean biogeographical boundaries determined using physical and biogeochemical variables[35]. Net growth period length ranges from less than two months in the Pacific equatorial biome (P_EQU) to more than three months in the high latitudes of the Northern Hemisphere such as the North Pacific and Atlantic subpolar seasonally stratified biome (NP_SPSS and NA_SPSS) and Northern Hemisphere ice biome (NH_ICE).

Projected future changes in the phenological features reveal a complex response pattern (Fig. 2a–c). Bloom initiation is expected to shift earlier in almost all biomes (Fig. 2a). In the Equatorial Pacific (P_EQU), the South Atlantic (SA_STPS, and SA_STSS), and parts of the Pacific sector of the Southern Ocean (SP_STSS), the timing of peak phytoplankton blooms are expected to be delayed by the end of the 21st century (Fig. 2b). For biomes over the remaining ocean regions, the bloom peak tends to occur earlier. The trends in peak bloom and initiation

times can be as large as one month over the 21st century. Resultant changes in the net growth period duration indicate that the ocean's "spring" can be shortened in the future to the north of 30°N and in the subpolar band of the Southern Ocean (Fig. 2c), with the shifts in initiation and peak timing exhibiting at least some degree of independence. This provides a first indication that drivers other than just temperature are playing an important role.

In contrast, future projected changes in peak amplitude reveal coherent spatial structures showing both increases and decreases in the magnitude of the bloom. Ensemble mean trends over 1990-2100 (Fig. 2d) reveal that peak bloom amplitudes are weakened in many regions. However, there are statistically significant increases over the subpolar North Pacific (NP_SPSS), the subtropical South Atlantic (NA_STSS and NA_STPS) and the Southern Ocean. This spatial pattern corresponds well with the trend in annual mean sea surface Chl evaluated previously with the same model configuration[21], indicating that intermittent blooms within the net growth period play an important role in determining the mean state trend. In the subtropical Indian Ocean and equatorial biomes, changes in the bloom penological features compensate for the changes in amplitude, i.e., the net growth period is longer, but its magnitude is smaller.

The time of emergence (ToE), considered as a signal-to-noise ratio, reveals that trends in ocean phytoplankton phenology are weakly emergent relative to trends in peak amplitude (Fig.2 and Fig.S2). The natural variability of the phenological features of blooms are as large as the forced response over many regions. For ecosystems, this ToE can also be interpreted to represent when the forced phenology changes exceed the envelope of ambient natural variability on a biome scale, potentially serving as a threshold for when phytoplankton phenology can sustain phenological mismatch and trophic asynchrony. Results from our analysis underscore the

challenges in detection of phenological changes from localized observations, as has been previously noted for seasonal amplitude modulations[17,36]. Nevertheless, the emergence characteristics of several specific regions warrant special mention. For the Northern Hemisphere ice biome (NH_ICE), with projected rapid ice cover retreat, net growth period compression emerges during the first half of the 21st century, with the earlier shift of peak bloom timing largely sustaining the early emergence in net growth period length (Fig. 1). Additionally, in a few regions (e.g., NP_SPSS, IO_EQU, and NA_SPSS), the phase shift emerges earlier than the amplitude change (Fig. S2), suggesting a higher potential future risk of occurrence of trophic mismatch.

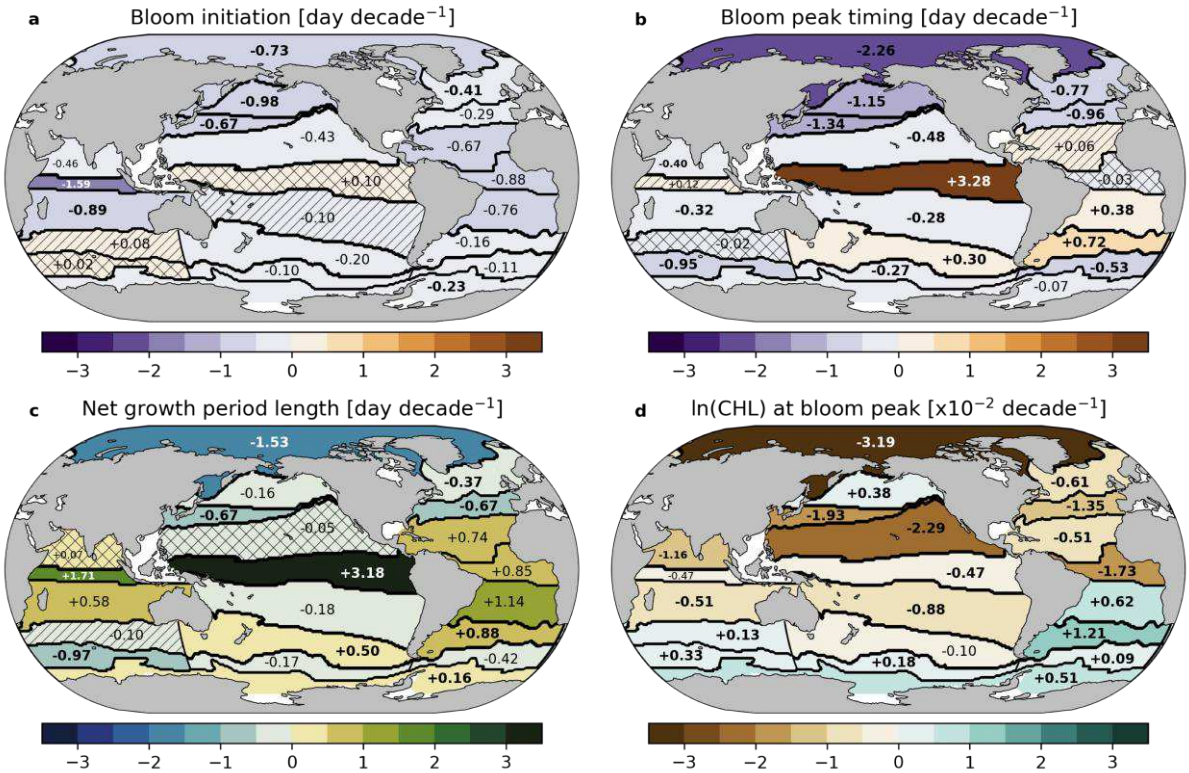


**Figure 2. Anthropogenic phenological shifts in both bloom initiation and peak bloom timing results in spatially diverse impacts on net growth period.** Ensemble mean trends (1990-2100) of (a) bloom initiation, (b) bloom peak timing (c) net growth period length, and (d) bloom magnitude over biomes. Positive trends indicate delay of initiation, delay of peak timing, extension of the net growth period, and increase in the bloom magnitude. Hatched (crosshatched) trends are statistically insignificant trends within the 99% (90%) confidence level. Trends indicated with bold numbers are emergent signals by the end of 21$^{st}$ century based

on time of emergence (ToE) calculation for the biome-aggregated time series. The ToEs are defined as the first year when the ensemble mean of the individual members' trends exceeds twice the ensemble standard deviation of those trends[21].

## Mechanistic drivers of phenological change

The normalized accumulation rate of Chl ($r$) is determined by the growth and loss of phytoplankton throughout the water column (including cell division, predation by zooplankton, aggregation, mortality, etc.), changes in Chl:C ($\theta$) (photoacclimation, the physiological response of phytoplankton), and a dilution effect due to surface mixed layer (ML) deepening,

$$r \equiv \frac{1}{chl}\frac{d\,Chl}{dt} \approx \mu - l + \frac{d\ln(\theta)}{dt} - \frac{d\ln(h)}{dt}, \quad (1)$$

where $h$ indicates the ML depth; $\mu$, $l$, are phytoplankton growth and loss rates; and $\frac{d\ln(\theta)}{dt}$ is the temporal changes in Chl:C summed over three phytoplankton groups, after weighting by each group's abundance (Equation M3 in Methods).

For a typical seasonal cycle in the subpolar North Atlantic, a focus of many observational studies, surface Chl begins to increase in late winter ($r$ becomes positive) and reaches its peak in early summer ($r$ becomes zero) (Fig. 3a, b). Projected future shifts to an earlier phytoplankton bloom initiation are characterized by a positive accumulation rate change ($\Delta r$; defined by future minus present day, Equation. M4) in late winter (Fig. 3b, c). Conversely, for the peak bloom timing, a positive (negative) $\Delta r$ between the present-day and future conditions represents a shift to a later (earlier) phasing (Fig. 3b, c). Budget analysis for the accumulation rate change shows that the dominant terms for the positive $\Delta r$ at bloom initiation are an increase in growth rate and increase in temporal variation of ML depth in January/February, while the earlier peak bloom timing (negative $\Delta r$) results from a reduced growth rate in May (Fig. 3c).

By further decomposing the growth rate changes into contributions from temperature, nutrient and light limitation (see Methods and Supplementary note for complete expressions), we can attribute variations in the bloom timing to changes in environmental drivers. This was accomplished by computing the coefficients of a Taylor expansion of the biogeochemical component of ESM2M (Methods). The change in the growth rate in January/February that sustains the earlier bloom initiation in the subpolar North Atlantic is mainly sustained by enhanced light availability (Fig. 3d). On the other hand, the negative changes in growth rate in May, which causes the earlier bloom peak, result from enhanced nutrient and temperature limitation (Fig. 3d). The subpolar North Atlantic is within the "warming hole" where the temperature trend is negative, in contrast to most other ocean regions[21], and thus, the bloom ends earlier, with peak timing shifted due to adverse conditions associated with reduced nutrient supply and colder temperatures.

The drivers of shifts in bloom initiation and peak often differ at the local scale (grid-cell) and across regions. For example, in the eastern subarctic North Pacific, surface warming is the major driver for both earlier bloom initiation and earlier bloom peak, by increasing growth rates at the bloom initiation and by increasing predation pressure (i.e., increase in loss rate) at the bloom peak, respectively (Fig. S3).

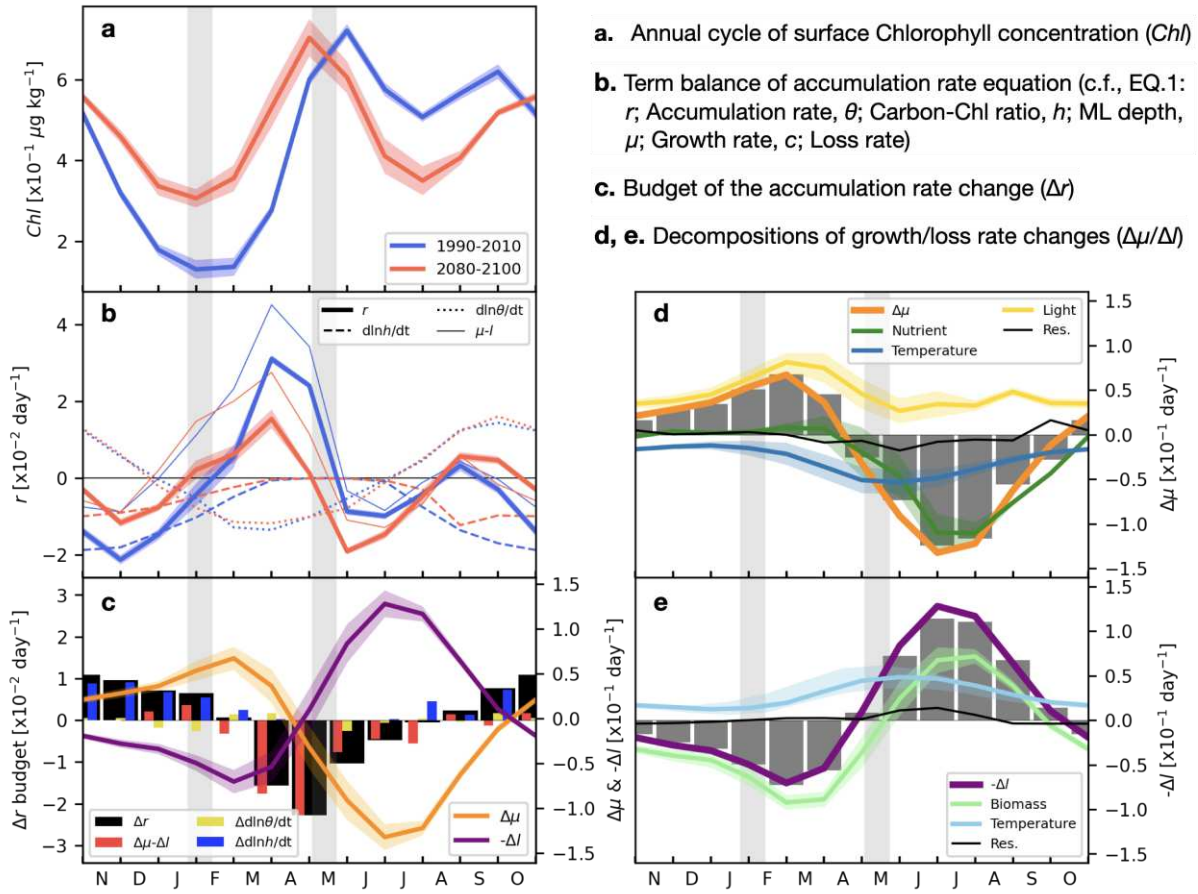


**Figure 3. Projected change in net growth period length and its driving processes revealed by the accumulation rate budget analysis in the North Atlantic (45°W, 55°N).** (a) Future (2080-2100, red lines) and present day (1990-2010, blue lines) annual cycle of the surface chlorophyll concentration. (b) Term balance of the accumulation rate equation (Equation 1); accumulation rate (solid thick lines with shades), growth/loss rate difference (solid thin line), ML depth variation (dashed lines) and Chl:C variation (dotted lines). (c) Accumulation rate changes (black bars, left axis) and the RHS terms from the accumulation rate budget (colored bars, left axis, Equation. M4). The growth and loss rate change are shown separately as lines with shading (right axis). (d, e) Decompositions of growth rate and loss rate change into changes in environmental drivers. Dark gray bars are the sum of all terms of the RHS of the Taylor decompositions (Equation. M5 and M6). Light gray shades in all panels indicate the bloom initiation/peak timing differences between present-day and future. All line shadings are the range of one standard deviation of 30 ensemble members.

## Regional differences of the dominant driver

The largest contributions to the accumulation rate budget for individual biomes are shown in Fig. 4, where we have estimated the relative contributions of the processes as the ratio of (i) the time integrated RHSs of Equation M4, to (ii) those of accumulation rate change (LHS in Equation M4), over the period between future and present-day bloom initiation/peak timing

241 (e.g., gray shaded periods in Fig. 3). In almost all ocean regions, contributions from changes
242 in growth and loss rates are the dominant terms of the accumulation rate changes that induce
243 bloom timing shifts (Fig. S5). The individual growth and loss rate changes are large enough
244 that each one alone could greatly alter the timing of the bloom peak. However, these two
245 contributions nearly mirror each other, reflecting the fact that phytoplankton growth and
246 predation by zooplankton are tightly coupled in this model. This compensation can be seen in
247 the analysis of the changes in the bloom initiation (Fig. S4). Previous studies have shown that
248 this tight coupling can be seen in observations and plays important role in explaining
249 climatological features of the phytoplankton bloom and its interannual variability[19,25].
250
251 While phytoplankton growth and loss rates are tightly coupled, there are slight differences of
252 the changes in growth and loss rate ($\Delta\mu - \Delta l$). This trophic level decoupling is the main
253 mechanism for the shift of the peak bloom timing and initiation in almost all ocean regions
254 (Fig. 4). In the oligotrophic mid-latitude ocean, the phytoplankton physiological response
255 (temporal changes in Chl:C) is often the secondary, or even primary, process sustaining shifts
256 in bloom peak timing, in agreement with previous results from observational and modeling
257 studies focused on interannual time scales[37]. Over parts of the Southern Ocean and the North
258 Atlantic, the dilution effect strongly alters bloom initiation, reflecting the large ML depth
259 changes in these regions by the end of the 21st century (Fig. S8c). The anti-correlation of the
260 contributions of temporal changes in ML depth and Chl:C (Fig. 4b, d, S4d, e and S5d, e) reflects
261 the physiology of photoacclimation, by which light-limited phytoplankton (i.e., deepening ML)
262 would increase their Chl:C.
263
264 Contributions of changes in environmental drivers, decomposed from growth/loss rate changes
265 in the bloom peak timing and initiation, reveal that each driver has distinct spatial footprints

(Fig S6 and S7), and the dominant driver over each ocean region also differs (Fig. 5). Bloom initiation often occurs earlier due to reduced light and temperature limitations on growth (except for IO_EQU). On the other hand, increased predation pressure (due to increase temperature and biomass abundance) can shift bloom peak timing earlier in many regions (e.g., NP_SPSS and SH_ICE), while enhanced growth rate (due to increased temperature) delays the bloom peak in others (e.g., SA_STSS and SA_STPS). In the Arctic Ocean (NH_ICE), where relatively early emergence of the change in the bloom phenology is identified, the main driver of the earlier initiation is enhanced light availability (Fig. 5a), as conceptually described in a previous study[38]. An earlier peak follows the earlier initiation, as the bloom will experience stronger predation pressure associated with abundance of phytoplankton biomass (Fig. 5b). As a result, despite the bloom starting earlier, the net growth period length is reduced due to larger shifts in the peak timing.

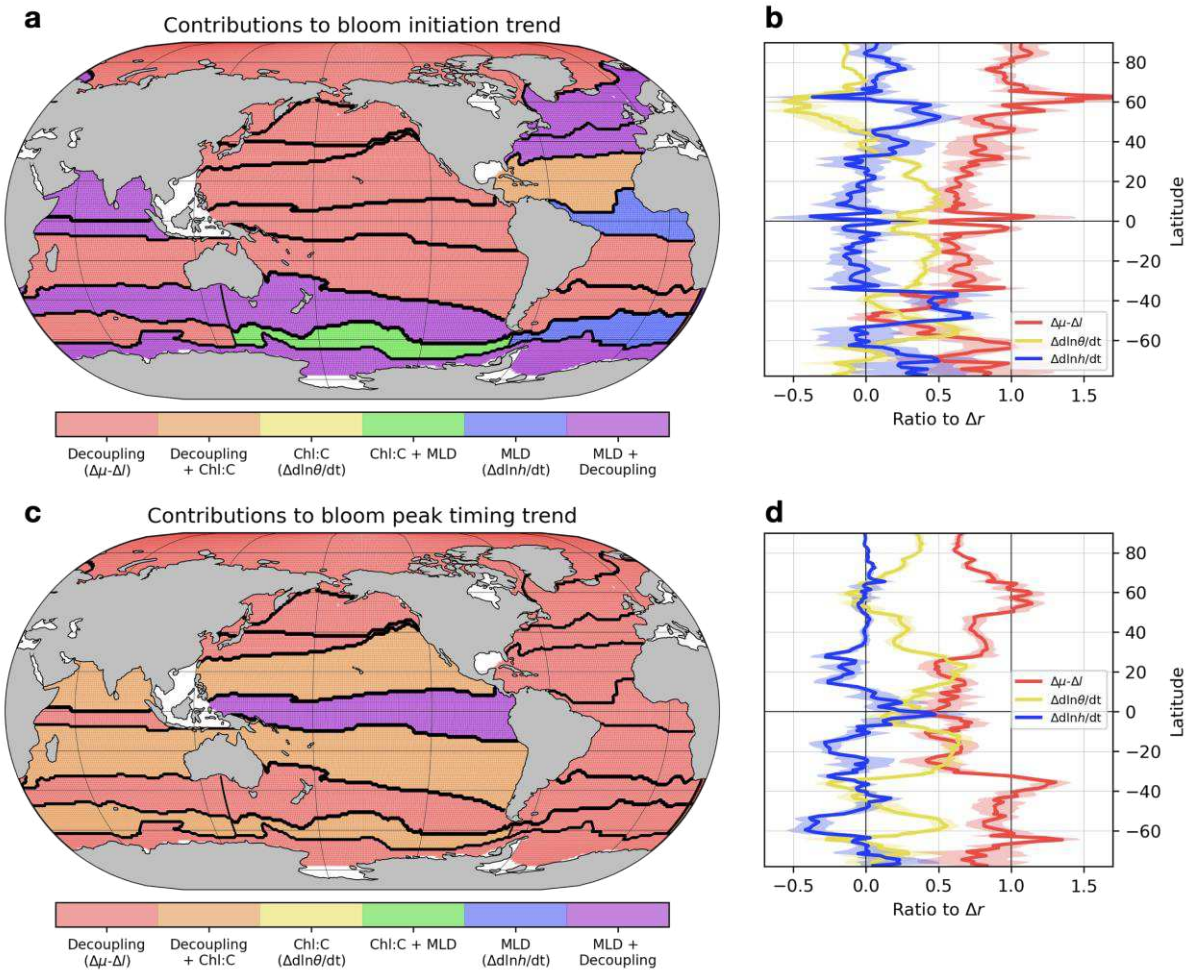


**Figure 4. Relative contributions of three driving processes of shifts in (a, b) bloom initiation and (c, d) bloom peak timing, through application of the accumulation rate budget analysis**. (a, c) Largest contribution(s) in each biome among decoupling of changes in growth and loss rate ($\Delta\mu - \Delta l$), change in ML depth variation ($\Delta\, d\ln(h)/dt$) and change in Chl:C variation ($\Delta\, d\ln(\theta)/dt$)). The largest contribution(s) in each biome indicate that the term dominantly contributes to accumulation rate change in more than 30 % area of the biome. (b, d) Zonally averaged relative contributions of three driving processes to the accumulation rate change. Line shadings indicates the range of one standard deviation of the 30 ensemble members.

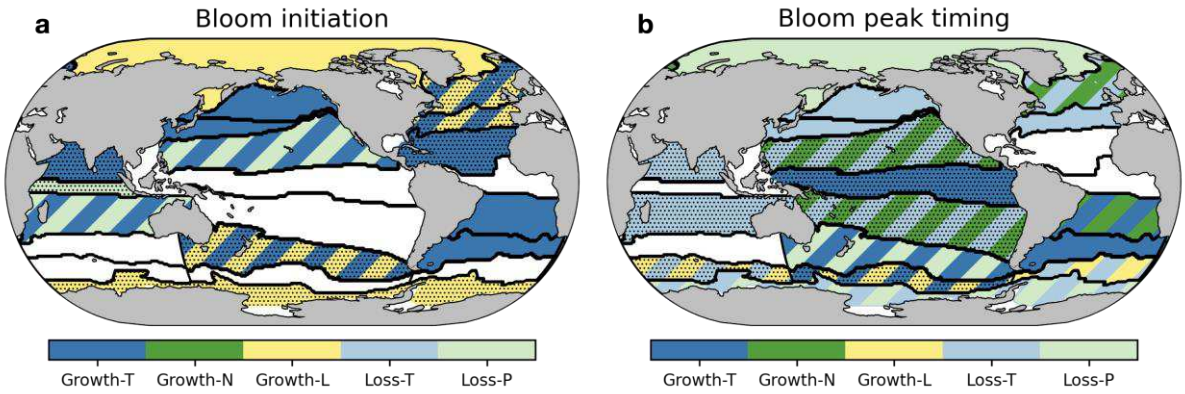


**Figure 5. Dominant environmental drivers of future phytoplankton growth and loss rate changes at (a) the bloom initiation and (b) bloom peak timing**. In the regions where the growth/loss rate change dominate the accumulation rate changes (Fig. 4), Growth-T, Growth-N, and Growth-L indicate that changes in temperature, nutrient, and light limitation, respectively, have the largest contribution to causing the growth/loss rate changes, that is, shifting the bloom timing. Similarly, Loss-T and Loss-P indicate that loss rate changes due to temperature and biomass abundance change, respectively, have largest contribution to shifting the timing. The dominant driver(s) in each biome indicate that the change in the driver dominates the growth/loss change in more than 20 % area of the biome. Dots superposed on biomes indicate regions where the other contributions (Chl:C variation changes or ML variation change) are comparable to the contribution from decoupling of growth/loss rate change in Fig. 4a and 4c. Dominant drivers in the biomes where these show statistically insignificant trends (Fig. 2a and 2b) and growth/loss rate change is not important (Fig. 4a and 4c) are not shown (white shading).

# Discussion

Overall, warming operates as a major driver for future shifts in both bloom initiation and peak timing, through changing growth and loss rates over most of the mid- to low latitudes and parts of the high latitudes (blue and light blue in Fig. 5). Thus, drivers of phytoplankton phenology shifts can be distinct from general nutrient limitation drivers of projected annual mean NPP changes over the same regions[30,39]. While phase shifts in bloom initiation are largely driven by changes in growth rates, increased predation pressure by zooplankton (top-down control) provide an important contribution to shifts in bloom peak timing over much of the global ocean. An implication with particular importance for observational studies is that bottom-up controls represent a necessary but not sufficient account for phenology changes, and that substantial roles for zooplankton and physiological responses of phytoplankton (Chl:C), which are

generally difficult to assess in observational studies, are a complementary and necessary component of a mechanistic account.

As our analytic framework is anchored in quantifying biomass accumulation budgets, we were able to deconvolve the underlying drivers, in contrast to simple correlation based analysis. Within this framework, our results indicate that the light-limitation mechanism for controlling bloom initiation at the heart of the Sverdrup hypothesis is only dominant over limited regions (Growth-L in Fig. 5a). Even there, light limitation changes are mediated not only through ML changes (i.e., enhanced stratification), but also through changes in incident solar radiation at the sea surface, with regional dependence (Fig. S8). As an example of the diversity of drivers identified here, the highly productive subarctic North Pacific and subpolar North Atlantic both exhibit earlier bloom initiation, but for different reasons. Whereas enhanced light availability is one of the main drivers for the shift in the subpolar North Atlantic, the main driver over the subarctic North Pacific is enhanced growth due to warming. As stratification changes are almost always concurrent with surface warming and enhanced light availability, these results underscore the inherent limitations of correlation-based diagnostics for quantitative attribution of changes in bloom initiation.

# Outlook

Our study identified substantial changes in marine phytoplankton phenology in a Large Ensemble conducted with an individual Earth system model (GFDL-ESM2M). The large ensemble enabled us to evaluate both the forced ocean biogeochemical response to climate change (signal) and the intrinsic background natural variability (noise), and thereby to also evaluate when such changes might robustly occur. The changes in the phytoplankton bloom initiation and peak timing, and the resulting changes in the net growth period length, are

349 spatially heterogenous. The spatial heterogeneity reflects a delicate balance between the
350 transient behavior of phytoplankton themselves and the individual underlying abiotic drivers,
351 resulting in the shifts in bloom timing in this model. Phytoplankton phenological changes are
352 weakly emergent over decadal timescales even after biome aggregation, indicating a stringent
353 need for sustained observations over multiple decades and over broad regions for detection of
354 secular trends. Nevertheless, model uncertainty of physical and ecological processes can be
355 large[40], and it is our hope that our study motivates further work to advance representation of
356 processes that sustain marine growing season characteristics.
357
358 Our main finding is that trophic level decoupling in response to anthropogenic forcing is the
359 main mechanism for both expanded and compressed future changes in net growth period length.
360 In high latitude regions, our results stand in contrast to the terrestrial biosphere, where
361 phenological changes are anticipated to shift more uniformly to expanded growing seasons as
362 a forced response to anthropogenic warming and $CO_2$ fertilization. This remarkable difference
363 reflects the fact that, in the ocean, warming sets in motion a number of interacting perturbations
364 that encompass both bottom-up and top-down drivers, with the balance between these drivers
365 playing out quite differently in different biome regions.
366
367 Since phytoplankton are crucial for fixing energy at the base of the food web, these results are
368 expected to have broad repercussions for ecosystem and food security through trophic
369 mismatches with the seasonal phasing of spawning in higher trophic levels[2]. Moreover, the
370 seasonal shifts in the timing of carbon fixation by phytoplankton are independent from shifts
371 in the seasonal cycle of temperature and mixing, which may have important consequences for
372 modulating ocean $CO_2$ uptake and ocean acidification. These results should motivate and

inform both observational and modeling efforts to explore the implications of phytoplankton changes for higher trophic levels and fisheries.

# Methods

## Model and observational data

The 30-member ensemble simulation used in this study was conducted with the Geophysical Fluid Dynamics Laboratory Earth System Model 2 (GFDL-ESM2M[31,32]) under historical (1950–2005) and RCP8.5 (2006–2010) pathways over 1950-2100. The initial conditions for individual ensemble members 2–30 (the 1 January 1950 conditions) were the chosen as the model state of the first ensemble member on January 2$^{nd}$ to 30$^{th}$, 1950. The model runs presented here share the initial conditions, model version, and forcing with the results presented by a previous study[33] but differ in that they were performed on a separate computing architecture and thereby differ member-by-member in their statistical (but not mean state) characteristics. The ocean biogeochemical component of the ESM2M (Tracers of Ocean Phytoplankton with Allometric Zooplankton code version 2; TOPAZ2) has three phytoplankton and one zooplankton groups and explicitly calculates a chlorophyll-caron ratio (CHL:C) from background light, nutrient, and temperature conditions. Comparison of ESM2M and other CMIP5 models with observations, in terms of the ocean biogeochemistry, has been documented for historical[41] and RCP8.5[42] simulations. We used daily means of surface Chl for detecting future changes in the bloom timing and monthly outputs of other ocean physical and biogeochemical fields for calculating the more extensive budgets over the time period of 1990–2100.

We also used a satellite-derived daily ocean surface Chl product[43] to validate model representations of phytoplankton bloom phenology (Fig. S1). Missing data due to cloud cover and the polar night are linearly interpolated along the time axis, except for the data gaps that lasts more than 14 days. All model and observational daily data are low-passed filtered by a Lanczos filter with a 20-day half power period before calculating the bloom timings, to remove

a transient spike response of the phytoplankton to atmospheric storm timescales and ocean mesoscale perturbations which are not the target of this study. In Fig. S1, to fairly compare the model data with the observations, we first resampled Chl from individual ensemble members using observational information of missing data grids. Subsequently, the same processing (linear interpolation and time filtering) was performed on the resampled model data and the following phytoplankton bloom metrics were computed. We wish to note that, with the exception of Figure S1, all analyses have been done without the resampling process in order to be consistent along the time-dimension of the model output from year 1990 to the end of the simulation (year 2100).

## Phytoplankton bloom definition

To calculate phytoplankton bloom initiation and peak timing, we apply the accumulation rate ($r \equiv \frac{d\ln(Chl)}{dt}$) based definition[27] for daily surface Chl data. We used the surface values rather than depth-averaged or depth-integrated values to be able to compare a broadly observable and well-established quantity provided by satellite measurements, although the total mixed layer Chl or phytoplankton biomass itself is a more appropriate metric for the representation of temporal variation[19]. In an annual cycle, the bloom initiation (peak) is defined as the time when the accumulation ratio becomes positive (negative) and the difference between the peak and the initiation gives net growth period length. To avoid artificial bloom timing jumps due to discontinuities in calendar dating, the annual cycle is defined as twelve months centered about the maximum day of climatological surface Chl in the annual calendar cycle at each grid point. We first obtain the peak timing within the annual cycle at each grid point with the natural logarithm of Chl time series. We then use the corresponding accumulation rate ($r$) time series to back-search for consecutive 14 day intervals with negative accumulation, representing a

non-bloom periods. We defined the transition from bloom periods (positive $r$) to non-bloom period (negative $r$) as the bloom initiation.

In the case that there are more than two peaks of surface Chl in an annual cycle, we chose the largest one to represent the bloom at the grid point. In a few ocean regions, blooms identified in our model analysis are thus different from the observed annual maximum bloom. For example, in the subpolar band of the Southern Ocean, the modeled annual maximum bloom occurs in autumn (greenish zonal band in the Southern Ocean in Fig. S1d), although in observations it is rather the spring bloom.

## Accumulation rate budget analysis

Under the assumption that Chl advection and diffusion terms are negligible over spatial and temporal scales of 100 km and 1 month, respectively, we start from the conservation equation for phytoplankton biomass ($P_i$) in the mixed layer;

$$\frac{dP_i h}{dt} = (\mu_i - l_i)\, P_i h, \qquad \text{(M1)}$$

to derive an equation for computing the budget of Chl, where $\mu$, $l$, and $h$ indicate the phytoplankton growth rate, loss rate, and ML depth, respectively, and the subscript $i$ represents phytoplankton groups in the model (small phytoplankton, large phytoplankton, and diazotroph). Subsequently, the conservation equation is rewritten as a vertical one-dimensional phytoplankton biomass equation[44,45],

$$\frac{dP_i}{dt} = (\mu_i - l_i)\, P_i - \frac{P_i}{h}\frac{dh}{dt}. \qquad \text{(M2)}$$

Assuming the water is well mixed within the ML, the biomass concentration at the surface is identical to the concentration averaged over the ML. Sea surface biomass concentration can vary with its growth (cell division) and its loss (zooplankton grazing, aggregation, mortality etc.) in the ML. Additionally, entrainment of biomass-free water from below through ML

deepening can dilute the ML biomass concentration. Here, the effect is parameterized as follows;

$$\frac{dh}{dt} = \begin{cases} \frac{dh}{dt} & \left(\frac{dh}{dt} > 0; deepening\right) \\ 0 & \left(\frac{dh}{dt} \leq 0; shoaling\right) \end{cases}.$$

Using the chlorophyll to carbon ratio ($\theta_i = \frac{Chl_i}{P_i}$), the phytoplankton biomass equation can be rewritten to the form of Equation (1) in the Main text,

$$\frac{d\ln(Chl)}{dt} \equiv r = \sum_{i=1}^{3}\left((\mu_i - l_i) + \frac{d\ln(\theta_i)}{dt}\right)\gamma_i - \frac{d\ln(h)}{dt}, \quad \text{(M3)}$$

where $Chl$ is the sum of the chlorophyll concentration of three groups ($chl = \sum_{i=1}^{3} Chl_i$), and $\gamma_i$ represents the concentration ratio of each group ($\gamma_i = Chl_i/Chl$). For convenience, in the Main text, summations of the changes in growth and loss rate, and Chl:C variations over the three phytoplankton groups are expressed without the subscript $i$.

Based on this equation, accumulation changes from present day to future ($\Delta r$) are described as the sum of four terms; change in growth rate, loss rate, time rate of change in the Chl:C, and time rate of change in the ML depth,

$$\begin{aligned} \Delta r &= \sum_{i=1}^{3}\Delta(\gamma_i\mu_i) + \sum_{i=1}^{3}\Delta(\gamma_i l_i) + \sum_{i=1}^{3}\Delta\left(\gamma_i\frac{d\ln(\theta_i)}{dt}\right) - \Delta\frac{d\ln(h)}{dt} \\ &\equiv \Delta\mu - \Delta l + \Delta\frac{d\ln(\theta)}{dt} - \Delta\frac{d\ln(h)}{dt}. \end{aligned} \quad \text{(M4)}$$

All terms in the accumulation rate budget analysis are calculated at individual grid points before aggregating across biomes.

# Decomposition of growth/loss rate change

In the TOPAZ2 biogeochemical component of GFDL-ESM2M, the phytoplankton growth rate is a function of temperature, nutrient, and light limitation terms ($T^{lim}$, $N^{lim}$, and $L^{lim}$), and the loss rate is described as a function of temperature limitation and the abundance of

phytoplankton biomass ($T^{lim}$ and $P_i$). Model parameters are assigned for each phytoplankton group and then the limitation terms are calculated separately so that the Taylor expansions of the total growth rate ($\Delta\mu$) and loss rate ($\Delta l$) are expressed as follow (See also supplementary note);

$$\Delta\mu = \sum_{i=1}^{3}\Delta(\gamma_i\mu_i) \approx \sum_{i=1}^{3}\gamma_i\frac{\partial\mu_i}{\partial T^{lim}}\Delta T^{lim} + \sum_{i=1}^{3}\gamma_i\frac{\partial\mu_i}{\partial L_i^{lim}}\Delta N_i^{lim} + \sum_{i=1}^{3}\gamma_i\frac{\partial\mu_i}{\partial L_i^{lim}}\Delta L_i^{lim} + \text{Residual}, \quad \text{(M5)}$$

$$\Delta l = \sum_{i=1}^{3}\Delta(\gamma_i l_i) \approx \sum_{i=1}^{3}\gamma_i\frac{\partial l_i}{\partial T^{lim}}\Delta T^{lim} + \sum_{i=1}^{3}\gamma_i\frac{\partial l_i}{\partial P_i}\Delta P_i + \text{Residual}. \quad \text{(M6)}$$

Residuals in the above equations include contributions from changes in the chlorophyll concentration ratio ($\gamma_i$) and other higher order terms, but tend to be minor overall (Fig. S6 and S7). Partial derivatives of the growth (loss) rate with respect to temperature, nutrient, and light limitation (temperature limitations and biomass) are computed analytically using model equations (Supplementary note).

# References (Up to 50 references (excluding those cited exclusively in Methods))


1. Kahru, M., Brotas, V., Manzano-Sarabia, M. & Mitchell, B. G. Are phytoplankton blooms occurring earlier in the Arctic?: PHYTOPLANKTON BLOOMS IN THE ARCTIC. *Global Change Biology* **17**, 1733–1739 (2011).
2. Asch, R. G., Stock, C. A. & Sarmiento, J. L. Climate change impacts on mismatches between phytoplankton blooms and fish spawning phenology. *Glob Change Biol* **25**, 2544–2559 (2019).
3. Edwards, M. & Richardson, A. J. Impact of climate change on marine pelagic phenology and trophic mismatch. *Nature* **430**, 881–884 (2004).
4. Palevsky, H. I. & Quay, P. D. Influence of biological carbon export on ocean carbon uptake over the annual cycle across the North Pacific Ocean: Influences on North Pacific Ocean $CO_2$ Uptake. *Global Biogeochem. Cycles* **31**, 81–95 (2017).
5. Signorini, S. R. *et al.* The role of phytoplankton dynamics in the seasonal and interannual variability of carbon in the subpolar North Atlantic – a modeling study. *Geosci. Model Dev.* **5**, 683–707 (2012).
6. Körtzinger, A. *et al.* The seasonal $p\,CO_2$ cycle at 49°N/16.5°W in the northeastern Atlantic Ocean and what it tells us about biological productivity. *J. Geophys. Res.* **113**, C04020 (2008).
7. Penuelas, J., Rutishauser, T. & Filella, I. Phenology Feedbacks on Climate Change. *Science* **324**, 887–888 (2009).
8. Ruosteenoja, K., Markkanen, T. & Räisänen, J. Thermal seasons in northern Europe in projected future climate. *Int J Climatol* **40**, 4444–4462 (2020).
9. Jeong, S.-J., Ho, C.-H., Gim, H.-J. & Brown, M. E. Phenology shifts at start vs. end of growing season in temperate vegetation over the Northern Hemisphere for the period

498 1982-2008: PHENOLOGY SHIFTS AT START VS. END OF GROWING SEASON.
499 *Global Change Biology* **17**, 2385–2399 (2011).
500 10. Zhou, B., Zhai, P., Chen, Y. & Yu, R. Projected changes of thermal growing season over
501 Northern Eurasia in a 1.5 °C and 2 °C warming world. *Environ. Res. Lett.* **13**, 035004
502 (2018).
503 11. Chen, M., Melaas, E. K., Gray, J. M., Friedl, M. A. & Richardson, A. D. A new seasonal-
504 deciduous spring phenology submodel in the Community Land Model 4.5: impacts on
505 carbon and water cycling under future climate scenarios. *Glob Change Biol* **22**, 3675–
506 3688 (2016).
507 12. Henson, S. A., Cole, H. S., Hopkins, J., Martin, A. P. & Yool, A. Detection of climate
508 change-driven trends in phytoplankton phenology. *Glob Change Biol* **24**, e101–e111
509 (2018).
510 13. Marchese, C. *et al.* Changes in phytoplankton bloom phenology over the North Water
511 (NOW) polynya: a response to changing environmental conditions. *Polar Biol* **40**, 1721–
512 1737 (2017).
513 14. Friedland, K. D. *et al.* Phenology and time series trends of the dominant seasonal
514 phytoplankton bloom across global scales. *Global Ecol Biogeogr* **27**, 551–569 (2018).
515 15. Tremblay, J.-É., Michel, C., Hobson, K. A., Gosselin, M. & Price, N. M. Bloom
516 dynamics in early opening waters of the Arctic Ocean. *Limnol. Oceanogr.* **51**, 900–912
517 (2006).
518 16. Winder, M. & Sommer, U. Phytoplankton response to a changing climate. *Hydrobiologia*
519 **698**, 5–16 (2012).
520 17. Henson, S., Cole, H., Beaulieu, C. & Yool, A. The impact of global warming on
521 seasonality of ocean primary production. *Biogeosciences* **10**, 4357–4369 (2013).

18. Hashioka, T., Sakamoto, T. T. & Yamanaka, Y. Potential impact of global warming on North Pacific spring blooms projected by an eddy-permitting 3-D ocean ecosystem model. *Geophysical Research Letters* **36**, (2009).
19. Behrenfeld, M. J. & Boss, E. S. Resurrecting the Ecological Underpinnings of Ocean Plankton Blooms. *Annu. Rev. Mar. Sci.* **6**, 167–194 (2014).
20. Behrenfeld, M. J. Climate-mediated dance of the plankton. *Nature Clim Change* **4**, 880–887 (2014).
21. Schlunegger, S. *et al.* Emergence of anthropogenic signals in the ocean carbon cycle. *Nat. Clim. Chang.* **9**, 719–725 (2019).
22. Sverdrup, H. U. On Conditions for the Vernal Blooming of Phytoplankton. *ICES Journal of Marine Science* **18**, 287–295 (1953).
23. Sommer, U. & Lewandowska, A. Climate change and the phytoplankton spring bloom: warming and overwintering zooplankton have similar effects on phytoplankton: WARMING, ZOOPLANKTON AND PHYTOPLANKTON SPRING BLOOM. *Global Change Biology* **17**, 154–162 (2011).
24. Behrenfeld, M. J. Abandoning Sverdrup's Critical Depth Hypothesis on phytoplankton blooms. *Ecology* **91**, 977–989 (2010).
25. Behrenfeld, M. J., Doney, S. C., Lima, I., Boss, E. S. & Siegel, D. A. Annual cycles of ecological disturbance and recovery underlying the subarctic Atlantic spring plankton bloom. *Global Biogeochem. Cycles* **27**, 526–540 (2013).
26. Arteaga, L. A., Boss, E., Behrenfeld, M. J., Westberry, T. K. & Sarmiento, J. L. Seasonal modulation of phytoplankton biomass in the Southern Ocean. *Nat Commun* **11**, 5364 (2020).
27. Behrenfeld, M. J. & Boss, E. S. Student's tutorial on bloom hypotheses in the context of phytoplankton annual cycles. *Glob Change Biol* **24**, 55–77 (2018).

28. Fu, W., Randerson, J. T. & Moore, J. K. Climate change impacts on net primary production (NPP) and export production(EP) regulated by increasing stratification and phytoplankton communitystructure in the CMIP5 models. *Biogeosciences* **13**, 5151–5170 (2016).
29. Kwiatkowski, L. *et al.* Twenty-first century ocean warming, acidification, deoxygenation, and upper-ocean nutrient and primary production decline from CMIP6 model projections. *Biogeosciences* **17**, 3439–3470 (2020).
30. Laufkötter, C. *et al.* Drivers and uncertainties of future global marine primary production in marine ecosystem models. *Biogeosciences* **12**, 6955–6984 (2015).
31. Dunne, J. P. *et al.* GFDL's ESM2 Global Coupled Climate–Carbon Earth System Models. Part II: Carbon System Formulation and Baseline Simulation Characteristics*. *Journal of Climate* **26**, 2247–2267 (2013).
32. Dunne, J. P. *et al.* GFDL's ESM2 Global Coupled Climate–Carbon Earth System Models. Part I: Physical Formulation and Baseline Simulation Characteristics. *Journal of Climate* **25**, 6646–6665 (2012).
33. Rodgers, K. B., Lin, J. & Frölicher, T. L. Emergence of multiple ocean ecosystem drivers in a large ensemble suite with an Earth system model. *Biogeosciences* **12**, 3301–3320 (2015).
34. Cabré, A., Shields, D., Marinov, I. & Kostadinov, T. S. Phenology of Size-Partitioned Phytoplankton Carbon-Biomass from Ocean Color Remote Sensing and CMIP5 Models. *Front. Mar. Sci.* **3**, (2016).
35. Fay, A. R. & McKinley, G. A. Global open-ocean biomes: mean and temporal variability. *Earth Syst. Sci. Data* **6**, 273–284 (2014).
36. Henson, S. A., Beaulieu, C. & Lampitt, R. Observing climate change trends in ocean biogeochemistry: when and where. *Glob Change Biol* **22**, 1561–1571 (2016).

572 37. Behrenfeld, M. J. *et al.* Revaluating ocean warming impacts on global phytoplankton.
573 *Nature Clim Change* **6**, 323–330 (2016).
574 38. Wassmann, P. & Reigstad, M. Future Arctic Ocean Seasonal Ice Zones and Implications
575 for Pelagic-Benthic Coupling. *Oceanog.* **24**, 220–231 (2011).
576 39. Nakamura, Y. & Oka, A. CMIP5 model analysis of future changes in ocean net primary
577 production focusing on differences among individual oceans and models. *J Oceanogr* **75**,
578 441–462 (2019).
579 40. Schlunegger, S. *et al.* Time of Emergence and Large Ensemble Intercomparison for
580 Ocean Biogeochemical Trends. *Global Biogeochem. Cycles* **34**, (2020).
581 41. Frölicher, T. L. *et al.* Dominance of the Southern Ocean in Anthropogenic Carbon and
582 Heat Uptake in CMIP5 Models. *Journal of Climate* **28**, 862–886 (2015).
583 42. Bopp, L. *et al.* Multiple stressors of ocean ecosystems in the 21st century: projections
584 with CMIP5 models. *Biogeosciences* **10**, 6225–6245 (2013).
585 43. NASA Ocean Biology Processing Group. MODIS-Aqua Level 3 Binned Chlorophyll
586 Data Version R2018.0. (2017) doi:10.5067/AQUA/MODIS/L3B/CHL/2018.
587 44. Behrenfeld, M. J., Doney, S. C., Lima, I., Boss, E. S. & Siegel, D. A. Reply to a comment
588 by Stephen M. Chiswell on: "Annual cycles of ecological disturbance and recovery
589 underlying the subarctic Atlantic spring plankton bloom" by M. J. Behrenfeld et al.
590 (2013): REPLY. *Global Biogeochem. Cycles* **27**, 1294–1296 (2013).
591 45. Llort, J., Lévy, M., Sallée, J.-B. & Tagliabue, A. Onset, intensification, and decline of
592 phytoplankton blooms in the Southern Ocean. *ICES Journal of Marine Science* **72**, 1971–
593 1984 (2015).
594
595
596

# Acknowledgements

R.Y., K.B.R., K.J.S., and A.T. were supported by the Institute for Basic Science (IBS), Republic of Korea, under IBS-R028-D1. S.S. acknowledges support by NSF's Southern Ocean Carbon and Climate Observations and Modeling (SOCCOM) Project under the NSF Award PLR-1425989, with additional support from NOAA and NASA. D.B. acknowledges support from NOAA under Ecosystem and Harmful Algal Bloom (ECOHAB) Award NA18NOS4780174. The authors thank to Dr. Hyung-Gyu Lim, Dr. Masao Ishii, and Dr. Katsuya Toyama for giving constructive comments on the analysis and manuscript. The analysis was conducted on the IBS/ICCP supercomputer "Aleph," 1.43 peta flops high-performance Cray XC50-LC Skylake computing system with 18,720 processor cores, 9.59 PB storage, and 43 PB tape archive space. High Performance Computing resources were also provided by NOAA Oceanic and Atmospheric Research/Geophysical Fluid Dynamics Laboratory.

# Author contributions

R.Y. and K.B.R. conceptualized the scientific framing of this study. R. Y. conducted all of the analysis and wrote the initial draft of the manuscript. R.Y., K.B.R., K.J.S., A.T., S.S., D.B., and J.P.D. contributed to development of the scientific ideas and the analytical methods, to interpretation of the results and contributed to writing the final draft of the manuscript. The simulations with the GFDL ESM2M were performed by S.S. and R.D.S., and post-processing was provided by K.B.R.

# Competing interests

The authors declare no competing interests.

## Supplementary Files

This is a list of supplementary files associated with this preprint. Click to download.

- 20210609suppbloomphenology.docx
- 20210609suppbloomphenology.docx